Journal of Engineering Mathematics **28**: 211–226, 1994.

Numerical solutions for the flow near the end of a shallow laterally heated cavity

P. WANG and P.G. DANIELS

Department of Mathematics, City University, Northampton Square, London, EC1V OHB, U.K.

Received 17 February 1993; accepted in revised form 13 August 1993

Abstract. The flow near the end of a shallow laterally heated cavity enters a nonlinear convective regime when the Rayleigh number R, based on cavity height, is of the same order of magnitude as the aspect ratio L (length/height). In the case of thermally insulated horizontal boundaries the end-region solution determines a correction to the flow and temperature fields throughout the cavity. Numerical solutions are obtained for the end-region flow for several different Prandtl numbers and for a range of values of the scaled Rayleigh number R/L using a Dufort-Frankel multigrid method. The results are compared with asymptotic predictions of the motion in the conductive limit $R/L \to 0$ and the boundary-layer limit $R/L \to \infty$.

1. Introduction

Flows driven by lateral heating in shallow rectangular cavities are of interest in relation to a number of physical and technological phenomena, including the production of crystals by the gradient-freeze technique (Hurle, Jakeman and Johnson [1]), cooling systems for nuclear reactors (Boyack and Kearney [2]), solar energy collectors (Bejan and Rossie [3]) and the dispersion of pollutants in river estuaries (Cormack, Leal and Imberger [4]). Experimental investigations of shallow cavity flows driven by lateral heating have been reported by Imberger [5], Bejan, Al-Homoud and Imberger [6] and Simpkins and Chen [7]. In a two-dimensional cavity the flow depends on three non-dimensional parameters, a Rayleigh number R, based on the cavity height and the lateral temperature difference, the Prandtl number of the fluid, σ and the aspect ratio of the cavity, L (length/height) which here is assumed to be large. For Rayleigh numbers $R \ll L$ the flow throughout the cavity consists of a Hadley cell driven by the constant horizontal temperature gradient set up between the end walls, [4]. Nonlinear convective effects first become significant in the turning motion near the ends when

$$R_1 = R/L = O(1)\,, \tag{1}$$

(Hart [8], Daniels, Blythe and Simpkins [9]). In the same range at sufficiently small Prandtl numbers the single Hadley cell becomes susceptible to a variety of instabilities (Hart [10]) and, above certain critical values $R_1 = R_{1c}$, the parallel core flow is replaced by multiple cells. The stationary transverse mode of instability actually forms an integral part of the basic steady motion in the cavity, appearing as an imperfect bifurcation of the nonlinear flow in the end regions. Solutions of the appropriate eigenvalue problem [9] suggest that in the case of thermally insulated horizontal boundaries this type of behaviour is relevant for Prandtl numbers $\sigma \leqslant 0.12$ and the ensuing motion is then difficult to treat analytically because nonlinear effects become important throughout the cavity for $R_1 > R_{1c}(\sigma)$. For larger Prandtl numbers, the asymptotic structure of the end-region solution as $R_1 \to \infty$ has been discussed by Daniels [11]. This limit is of particular significance because of the high Rayleigh numbers

encountered in practical applications and also because it represents an important step in the understanding of flow structures in square cavities where a horizontal boundary-layer structure consistent with the core and vertical boundary-layer motion proposed by Gill [12] remains undetermined. One of the difficulties is the unknown significance of the so-called 'mass-flux hypothesis' which assumes that all the fluid descending near the cold wall and ascending near the hot wall is expelled into the core before reaching the end of the vertical boundary layer. In the boundary-layer structure proposed in [11] for the limiting form of the end-region solution as $R_1 \to \infty$, all of the fluid entrained by vertical boundary layers is expelled into wall jets on the horizontal surfaces of the cavity. The balance of heat flux in the end regions also involves an unexpectedly large constant contribution to the local temperature field. One means of investigating whether the asymptotic structure does indeed possess these features is to solve the nonlinear end-region problem numerically.

In the present paper a Dufort-Frankel multigrid method is used to obtain numerical solutions of the end-region problem for several values of the Prandtl number σ and for a range of values of the scaled Rayleigh number R_1. The results are compared with the asymptotic predictions obtained in [4] for the conductive limit $R_1 \to 0$ and with the boundary-layer model proposed in [11] for the convective limit $R_1 \to \infty$. The end-region problem is formulated in Section 2 and in Section 3 the main results of the asymptotic analysis are summarised. The numerical method used to obtain solutions of the nonlinear Oberbeck-Boussinesq system is outlined in Section 4. Steady-state solutions are found by allowing the system to evolve in time from an appropriate initial configuration. A Dufort-Frankel method (Roache [13]) is used to solve the evolution equations for the thermal field and the vorticity field, while a multi-level method (Brandt [14]) is used to relate the stream function and vorticity fields via the solution of Poisson's equation. Results are obtained in Section 5 for three values of the Prandtl number, $\sigma = 0.05$, $\sigma = 0.733$ (air) and $\sigma = 6.983$ (water). In the first case the flow is subject to instability above the appropriate critical value R_{1c}, as in similar low Prandtl number calculations reported in [8] and here results are limited to $R_1 \leqslant 600$. Most calculations were performed for air, and results are obtained for values of R_1 up to 20 000, enabling a realistic comparison to be made with the predictions of the boundary-layer analysis. The results are discussed in Section 6.

2. Shallow cavity flow $R_1 = O(1)$

A cavity of length l and height h occupies the region $0 \leqslant x \leqslant L$, $0 \leqslant z \leqslant 1$ where (x, z) are cartesian coordinates nondimensionalised with respect to h. The cavity is filled with a fluid of kinematic viscosity ν, thermal diffusivity κ and coefficient of thermal expansion α. The end wall at $x = L = l/h$ is maintained at a constant temperature ΔT in excess of that at $x = 0$ and the two horizontal walls $z = 0$ and $z = 1$ are perfectly insulated. In the Oberbeck-Boussinesq approximation time-dependent motion is governed by the equations

$$\sigma^{-1}\left(\frac{\partial \bar{\omega}}{\partial t} + \frac{\partial(\bar{\omega}, \bar{\psi})}{\partial(x, z)}\right) = \nabla^2 \bar{\omega} + R\frac{\partial \bar{T}}{\partial x}, \tag{2}$$

$$\nabla^2 \bar{\psi} = -\bar{\omega}, \tag{3}$$

$$\frac{\partial \bar{T}}{\partial t} + \frac{\partial(\bar{T}, \bar{\psi})}{\partial(x, z)} = \nabla^2 \bar{T}, \tag{4}$$

for the vorticity $\bar{\omega}$, stream function $\bar{\psi}$ and temperature $\bar{T}$, which are non-dimensionalised with respect to κ/h^2, κ and ΔT respectively. The time t is non-dimensionalised with respect to h^2/κ and the Rayleigh number R and Prandtl number σ are defined by

$$R = \alpha g \, \Delta T h^3/\kappa\nu, \qquad \sigma = \nu/\kappa \,, \tag{5}$$

where g is the acceleration due to gravity. The boundary conditions on the rigid walls of the cavity are

$$\bar{\psi} = \frac{\partial \bar{\psi}}{\partial x} = \bar{T} = 0 \qquad \text{on } x = 0 \,, \tag{6}$$

$$\bar{\psi} = \frac{\partial \bar{\psi}}{\partial x} = 0 \,, \quad \bar{T} = 1 \qquad \text{on } x = L \,, \tag{7}$$

$$\bar{\psi} = \frac{\partial \bar{\psi}}{\partial z} = \frac{\partial \bar{T}}{\partial z} = 0 \qquad \text{on } z = 0, 1 \tag{8}$$

and it is easily verified that the governing equations and boundary conditions are consistent with Gill's [12] centro-symmetry relations

$$\left.\begin{aligned} \bar{\psi}(x, z, t) &= \bar{\psi}(L - x, 1 - z, t) \,, \\ \bar{T}(x, z, t) &= 1 - \bar{T}(L - x, 1 - z, t) \,, \end{aligned}\right\} \tag{9}$$

which, for appropriate initial conditions, effectively allow only one half of the flow domain to be considered.

The formal asymptotic structure of the steady flow in a shallow cavity where $L \gg 1$ and $R_1 = R/L = O(1)$ is described in [9]. Throughout most of the cavity (the core region) the solution satisfying (8) and (9) is dominated by the lateral conduction associated with a Hadley circulation, so that

$$\bar{T} = \xi + L^{-1}\left\{\left(\xi - \frac{1}{2}\right) C_1(R_1, \sigma) + R_1 F(z)\right\} + O(L^{-2}) \,, \tag{10}$$

$$\bar{\psi} = R_1\{1 + L^{-1} C_1(R_1, \sigma) F'(z)\} + O(L^{-2}) \,, \tag{11}$$

as $L \to \infty$, where $\xi = x/L$,

$$F(z) = \frac{1}{120} z^5 - \frac{1}{48} z^4 + \frac{1}{72} z^3 - \frac{1}{1440} \tag{12}$$

and $C_1(R_1, \sigma)$ is a constant contribution determined by matching with solutions near the end walls.

Near the cold wall, the solution adjusts to the boundary conditions (6) in a square zone where $x, z = O(1)$,

$$\bar{T} = L^{-1} T(x, z, t) + \cdots \,, \; \bar{\psi} = \psi(x, z, t) + \cdots \,, \; \bar{\omega} = \omega(x, z, t) + \cdots \,, \; (L \to \infty) \,, \tag{13}$$

and substitution into (2)–(4) indicates that a steady-state solution of the system

$$\sigma^{-1}\left(\frac{\partial \omega}{\partial t}+\frac{\partial(\omega, \psi)}{\partial(x, z)}\right)=\nabla^2 \omega+R_1 \frac{\partial T}{\partial x}, \tag{14}$$

$$\nabla^2 \psi=-\omega, \tag{15}$$

$$\frac{\partial T}{\partial t}+\frac{\partial(T, \psi)}{\partial(x, z)}=\nabla^2 T, \tag{16}$$

is required. From (6), (7) these equations are to be solved subject to

$$\psi=\frac{\partial \psi}{\partial x}=T=0 \qquad \text{on } x=0, \tag{17}$$

$$\psi=\frac{\partial \psi}{\partial z}=\frac{\partial T}{\partial z}=0 \qquad \text{on } z=0, 1 \tag{18}$$

and to match with the core solution

$$T \sim x+c+R_1 F(z), \ \psi \rightarrow R_1 F'(z), \quad x \rightarrow \infty. \tag{19}$$

The core temperature is determined to order L^{-1} through the matching requirement

$$C_1=-2c, \tag{20}$$

but the value of c itself can only be determined by solving the end-zone problem (14)–(19). At low Prandtl numbers ($\sigma \leqslant 0.12$) the behaviour (19) is only possible for values of R_1 less than a critical value R_{1c} (see [8], [9]) but otherwise steady-state solutions are expected to exist for any value of R_1. The aim of the present work is to determine such solutions numerically for a range of values of the two non-dimensional parameters σ and R_1.

3. Asymptotic properties of the steady-state end-zone solution

(i) $R_1 \rightarrow 0$

For small values of the scaled Rayleigh number R_1 the cavity flow is conduction-dominated everywhere and in the end region the temperature and stream function fields can be expanded in the form

$$T=x+R_1 T_1+R_1^2 T_2+\cdots, \tag{21}$$

$$\psi=R_1 \psi_1+R_1^2 \psi_2+\cdots. \tag{22}$$

Here ψ_1 is a solution of the inhomogeneous biharmonic equation $\nabla^4 \psi_1=1$ with appropriate boundary conditions obtained from (17)–(19), representing a symmetric turning motion in the end zone. Further terms $T_1, \psi_2, T_2, \ldots$ in the expansions (21), (22) are obtained in succession and have been calculated in [4]. Since T_1 is an odd function of z, the leading contribution to c arises from T_2, giving

$$c \sim 1.74 \times 10^{-6} R_1^2, \quad R_1 \rightarrow 0. \tag{23}$$

(ii) $R_1 \to \infty$

The main features of the boundary-layer structure proposed in [11] are as follows. Near the cold wall there is a vertical boundary layer where

$$T \sim R_1^{7/5} c_0 g(\eta), \quad \psi \sim R_1^{3/5} c_0^{1/4} (1-z)^{3/4} f(\eta), \quad R_1 \to \infty, \tag{24}$$

with $\eta = c_0^{1/4} R_1^{3/5} x/(1-z)^{1/4}$ and where f and g are the solutions of the system

$$\left.\begin{aligned} &f''' + \sigma^{-1}\left(\frac{3}{4} ff'' - \frac{1}{2} f'^2\right) - g + 1 = 0, \\ &g'' + \frac{3}{4} fg' = 0, \\ &f = f' = g = 0 \ (\eta = 0); \quad g \to 1, f' \to 0 \ (\eta \to \infty) \end{aligned}\right\} \tag{25}$$

equivalent to the similarity solution for the boundary layer on a heated vertical wall discussed by Pohlhausen [15]. Numerical solutions of (25) have been obtained by Ostrach [16] and, in particular, the wall heat transfer can be approximated to 0.5% by the formula

$$\lambda = g'(0) = \frac{3}{4} \sigma^{1/4} (2.436 + 4.884\sigma^{1/2} + 4.952\sigma)^{-1/4} \tag{26}$$

The parameter $c_0 = c_0(\sigma)$ which appears in (24) provides the limiting form of the temperature at the edge of the vertical boundary layer and can be determined by the fact that the steady-state heat flux

$$\int_0^1 \left(\frac{\partial T}{\partial x} + \psi \frac{\partial T}{\partial z}\right) \mathrm{d}z = Q \tag{27}$$

is independent of x at any station across the end zone. The large x form (19) implies that $Q = R_1^2 Q_0 + 1$ where $Q_0 = 1/362880$ and comparison with the value of Q implied by the heat transfer through the cold wall requires that

$$c_0 = (3Q_0/4\lambda)^{4/5} \tag{28}$$

The value of c_0 determines the constant leading order temperature at the edge of the vertical boundary layer, given by (24) as $R_1^{7/5} c_0$. Since this is larger than order R_1 it must form part of the constant term c in the outer form of T as $x \to \infty$ given by (19). Thus

$$c \sim R_1^{7/5} c_0(\sigma), \quad R_1 \to \infty. \tag{29}$$

The vertical boundary layer is driven by buoyancy associated with the lateral temperature gradient across the layer which is in turn needed to maintain the necessary heat flux balance. The layer entrains fluid and transports it to the bottom of the cold wall where it is expelled along the bottom surface of the end zone in the form of a wall jet whose structure has been considered by Daniels and Gargaro [17, 18]. The overall end-zone structure also involves the recirculation of fluid forced into the end zone by the parallel core flow. The mass flux of order R_1 implied by the velocity profile associated with (19) is larger than the flux within the vertical boundary layer and the main turning motion is believed to occur on two main lateral scales, a long scale $x \sim R_1$ governed by the horizontal boundary-layer equations and a

shorter scale $x \sim 1$ where the motion is primarily inviscid. The extent of the horizontal boundary-layer region can be estimated from the eigenvalue analysis presented in [9] and for infinite Prandtl number this gives an e-folding decay length

$$x \sim 2.20 \times 10^{-4} R_1 . \tag{30}$$

The existence of both short and long lateral scales, of order $R_1^{-3/5}$ and order R_1, as $R_1 \to \infty$ means that the accurate computation of high Rayleigh number flows in the end region is not straightforward. Here computations are limited to the range $R_1 \leqslant 20\,000$.

4. Numerical method

The end region problem (14)–(19) was solved numerically using a finite difference method. It was decided to employ an explicit method based on the Dufort–Frankel scheme outlined in [13] to follow the evolution of the system, in preference to an implicit method. Methods of the latter type (for example Crank and Nicolson [19], Peaceman and Rachford [20]) have the advantage of unconditional stability, allowing a large time step to be used, but involve the solution of large matrix systems at each time step. Like these methods, the Dufort-Frankel method has second order accuracy and although it must meet a Courant condition to maintain numerical stability (Drummond [21]), it involves significantly less computational time at each time step. The vorticity and heat equations are discretised using the Dufort-Frankel scheme with the Arakawa [22] representation of the Jacobian terms and a five-point multigrid scheme [14] is used to solve the Poisson equation for the stream function. The outer form (19) is handled by a finite truncation of x so that the conditions

$$\frac{\partial T}{\partial x} = 1 , \quad \psi = R_1 F'(z) \tag{31}$$

are applied in the computational domain at $x = x_\infty < \infty$. Further details are given by Wang [23].

The overall scheme of computation for a given Rayleigh number and Prandtl number can be described as follows. An initial state was usually taken either in the form of a conductive solution with no motion $T = x$, $\psi = \omega = 0$ $(0 \leqslant x < x_\infty)$ or in the form of a steady-state solution obtained at a lower Rayleigh number R_1. The temperature, vorticity and stream function fields are then found in succession at each time step, using an implicit scheme with successive over-relaxation for the first time step and then the Dufort-Frankel three-layer scheme for subsequent time steps. The computation continues until a steady-state solution is achieved, as measured by the maximum differences between successive values of T and ω. During the computation the heat-flux integral (27) is used to monitor the accuracy of the converged steady-state solution by calculating its value at several x stations and comparing with the known value of Q.

The computer code was checked by using it to find a numerical solution for the thermally-driven flow in a square cavity, replacing the outer boundary condition by $T = 1$ at $x = 1$. Results were found for a Rayleigh number $R_1 = 14660$ and Prandtl number $\sigma = 0.733$ using 10×10, 20×20, 30×30 and 40×40 computational grids and were found to be in good agreement with those obtained for the same problem by Cormack, Leal and Seinfeld [24], Kublbeck, Merker and Straub [25] and Drummond [21]. The results also agreed well with

those predicted by the Harwell code Flow3D. Values of the stream function at the centre of the cavity were found to differ by only 0.3% for the 30×30 and 40×40 grids.

5. Results

Low Prandtl number calculations were carried out with $\sigma = 0.05$ and Rayleigh numbers R_1 varying from 200 to 600. An outer boundary $x_\infty = 6$ and a 180×30 computational grid were used. For $R_1 = 200$ the flow remains parallel throughout most of the domain and a near-symmetric turning motion is limited to the region $0 \leqslant x \leqslant 1.5$. At $R_1 = 400$ the flow field exhibits closed streamlines with an eddy centred at $x \approx 1.5$, $z = 0.5$ and as the Rayleigh number increases, further eddies become evident along the centre-line $z = 0.5$, resulting in the flow pattern shown in Figure 1 for $R_1 = 600$. This behaviour is consistent with the onset of secondary flow predicted by a linear stability analysis of the parallel core flow, [10], [9], which suggests that the parallel flow will give way to stationary multicellular convection when R_1 reaches a value $R_{1c}(0.05) \approx 610$. The critical wavenumber of the instability is given by 2.65 and the corresponding critical wavelength $2\pi/2.65 = 2.37$ compares well with the distance 2.39 measured between the centres of neighbouring cells in Figure 1. The development of the instability can also be seen in plots of the skin friction on the bottom wall of the cavity, shown in Figure 2. Once the Rayleigh number exceeds its critical value it is no longer appropriate to apply the outer boundary conditions in the form (19) and the end region can no longer be considered in isolation. The local Nusselt number at the cold wall,

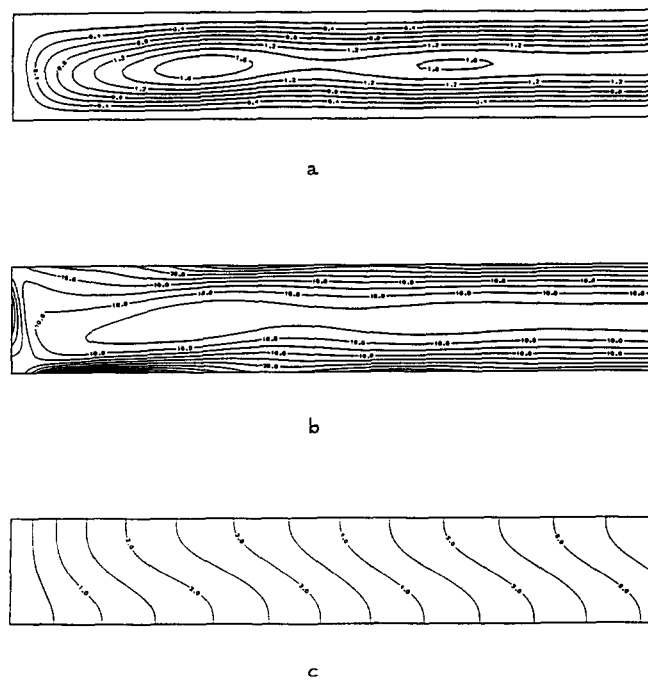

Fig. 1. Contours of the steady-state solution for (a) stream function, (b) vorticity, (c) temperature, for $\sigma = 0.05$ and $R_1 = 600$, using a 180×30 grid with $x_\infty = 6$.

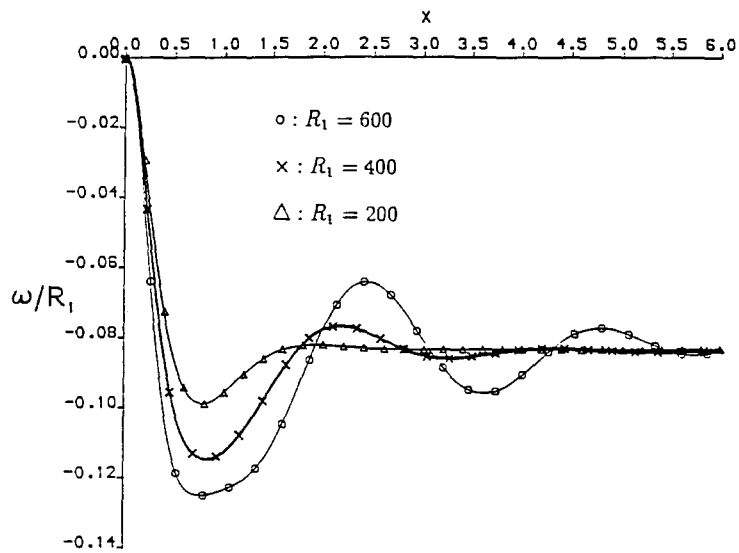

Fig. 2. Skin friction ω/R_1 on the bottom wall with $\sigma = 0.05$ for various Rayleigh numbers.

$$Nu = \left.\frac{\partial T}{\partial x}\right|_{x=0}, \tag{32}$$

is shown in Figure 3. Generally, the results obtained here are consistent with those obtained earlier in [8] and also with numerical simulations of the full cavity flow by Drummond and Korpela [26].

Extensive numerical calculations were carried out for air ($\sigma = 0.733$) where, in principle, a steady-state solution should exist for all Rayleigh numbers. Accurate results (as measured by the heat flux constraint (27)) were obtained for $100 \leqslant R_1 \leqslant 14\,000$ and further results with somewhat less accuracy for $R_1 = 20\,000$ and are summarised in Figures 4–10. Outer boundaries varying from $x_\infty = 3$ at the lowest Rayleigh number to $x_\infty = 20$ at the highest

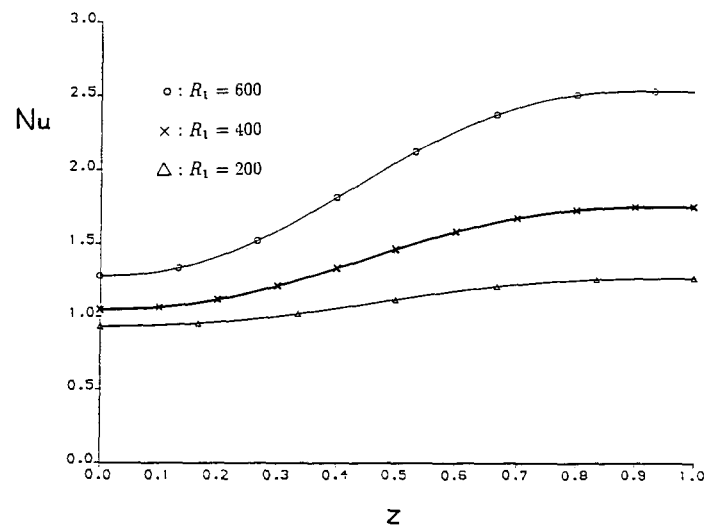

Fig. 3. Local Nusselt number Nu on the cold wall with $\sigma = 0.05$ for various Rayleigh numbers.

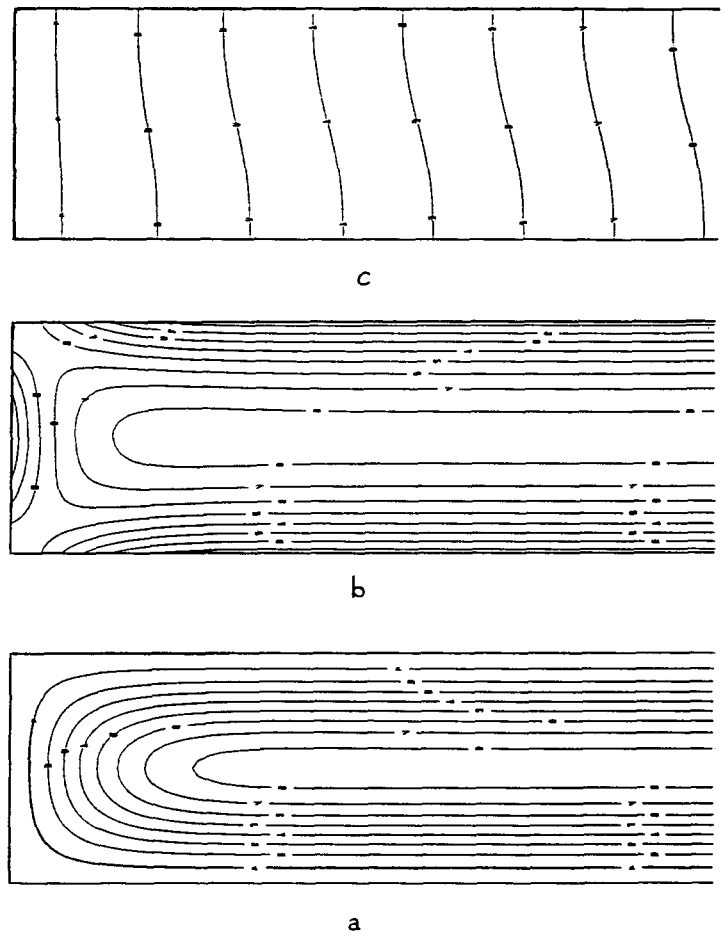

Fig. 4. Contours of the steady-state solution for (a) stream function, (b) vorticity, (c) temperature, for $\sigma = 0.733$ and $R_1 = 100$, using a 120×40 grid with $x_\infty = 3$.

Rayleigh number were used, with typical computational grids 90×30, 120×40, 150×25 and 175×25. It was found vital to increase the outer boundary in line with the type of behaviour made evident by (30) – failure to apply the outer boundary condition at a sufficiently large value of x led to the onset of numerical instability near x_∞. Figures 4–7 show streamlines, isotherms and vorticity contours.

For low Rayleigh numbers, roughly less than 1000 (Figures 4, 5) non-parallel flow is restricted to a square area near the cold wall, and away from that the flow is approximately parallel to the horizontal boundaries. For $R_1 = 100$ the flow is virtually symmetric and dominated by conduction, as expected from (21), (22). When R_1 increases to 5000 or more (Figures 6, 7) the flow patterns change dramatically. A vertical thermal boundary layer is gradually formed on the cold wall, with a horizontal width $x \ll 1$, while away from the cold wall the flow requires an increasingly large distance $x \gg 1$ to achieve the outer form associated with the parallel core flow. At the higher Rayleigh numbers the vertical boundary layer is much thinner, and the strongest horizontal temperature gradients are set up near the top corner of the cold wall, where there is vigorous convection down the wall. Also, a small eddy develops in the streamline field near the lower cold corner ($R_1 = 14\,000$, Figure 7) and

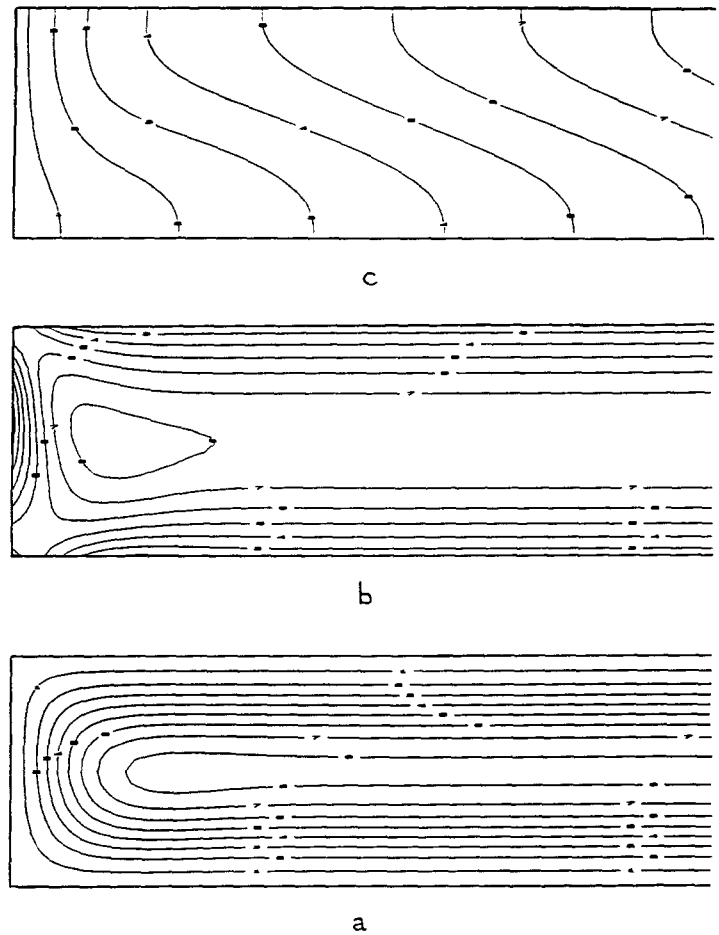

Fig. 5. Contours of the steady-state solution for (a) stream function, (b) vorticity, (c) temperature, for $\sigma = 0.733$ and $R_1 = 1000$, using a 90×30 grid with $x_\infty = 3$.

the flow diverges slightly from the lower horizontal boundary, consistent with a theoretical analysis of a possible horizontal boundary layer structure there in the limit $R_1 \to \infty$, [17, 18]. The isotherms descending the cold wall follow the streamlines near the base of the wall, indicating that the flow there is convectively-dominated at large Rayleigh numbers. Note also that most of the mass flux in the vertical boundary layer is conveyed to the base of the layer, consistent with the similarity solution of Section 3.

The skin friction and temperature on the bottom wall of the cavity are shown for different Rayleigh numbers in Figures 8 and 9. The skin friction develops both minimum and maximum values in the range $0 < x < 1$ before a constant asymptotic form is eventually attained as $x \to \infty$. This behaviour is associated with the complex flow near the bottom of the cold wall and suggests the possibility of flow separation on the bottom wall for Rayleigh numbers greater than 20 000. At large Rayleigh numbers an increasingly long scale in x is needed for the temperature to adjust to the linear conductive form associated with the parallel core flow.

Quantitative comparisons were made with the asymptotic structure outlined in Section 3 in three areas, relating to the form of the parameter $c(R_1, \sigma)$ as $R_1 \to \infty$ and to specific properties of the vertical boundary-layer solution. Figure 10 shows the computed values of c

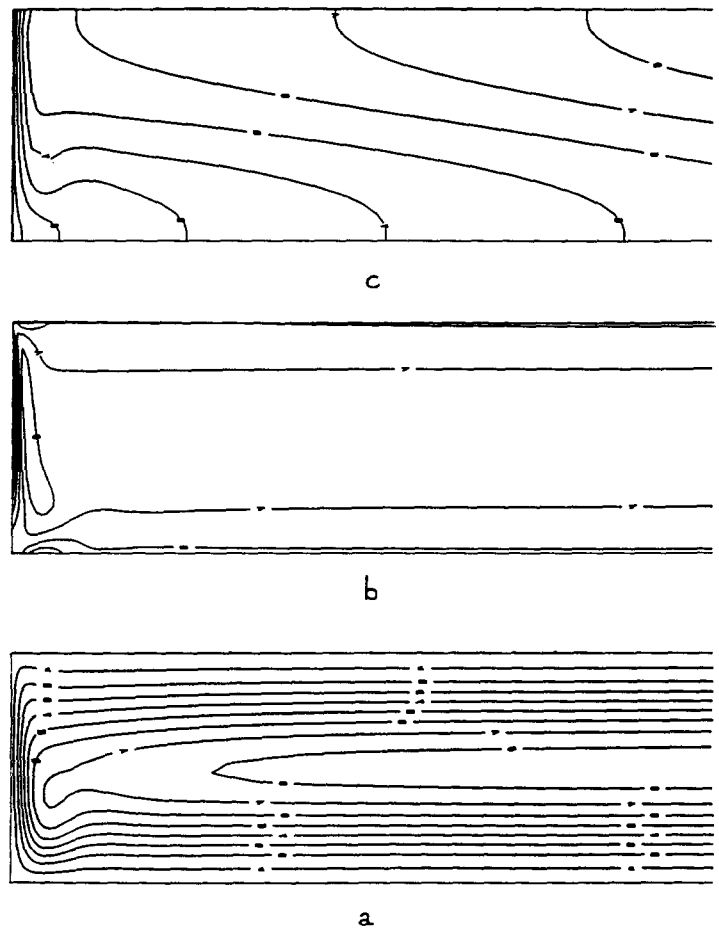

Fig. 6. Contours of the steady-state solution for (a) stream function, (b) vorticity, (c) temperature, for $\sigma = 0.733$ and $R_1 = 5000$, using a 150×25 grid with $x_\infty = 3$.

c based on the temperature profile (19) obtained in the numerical solution at x_∞. According to (29) the quantity $c/R_1^{7/5}$ should approach the constant limit $c_0(\sigma)$ as $R_1 \to \infty$ where, from (26) and (28), for $\sigma = 0.733$,

$$c_0 = 6.044 \times 10^{-5} . \tag{33}$$

This horizontal asymptote is shown in Figure 10 and is in good agreement with the numerical solution. At low Rayleigh numbers the asymptotic form (23) is also in excellent agreement with the numerical solution for $R_1 = 100$ where it was found that $c = 1.617 \times 10^{-2}$; the value predicted by (23) is $c = 1.74 \times 10^{-2}$.

Figures 11 and 12 show comparisons of the vertical boundary-layer structure for $R_1 \gg 1$ outlined in Section 3 with the numerical results. The boundary-layer theory predicts that the skin friction on the cold wall should approach a form proportional to $R_1^{9/5}$ as $R_1 \to \infty$, or more specifically,

$$R_1^{-9/5} \left. \frac{\partial w}{\partial x} \right|_{x=0} \to -c_0^{3/4}(1-z)^{1/4} f''(0) , \quad R_1 \to \infty , \tag{34}$$

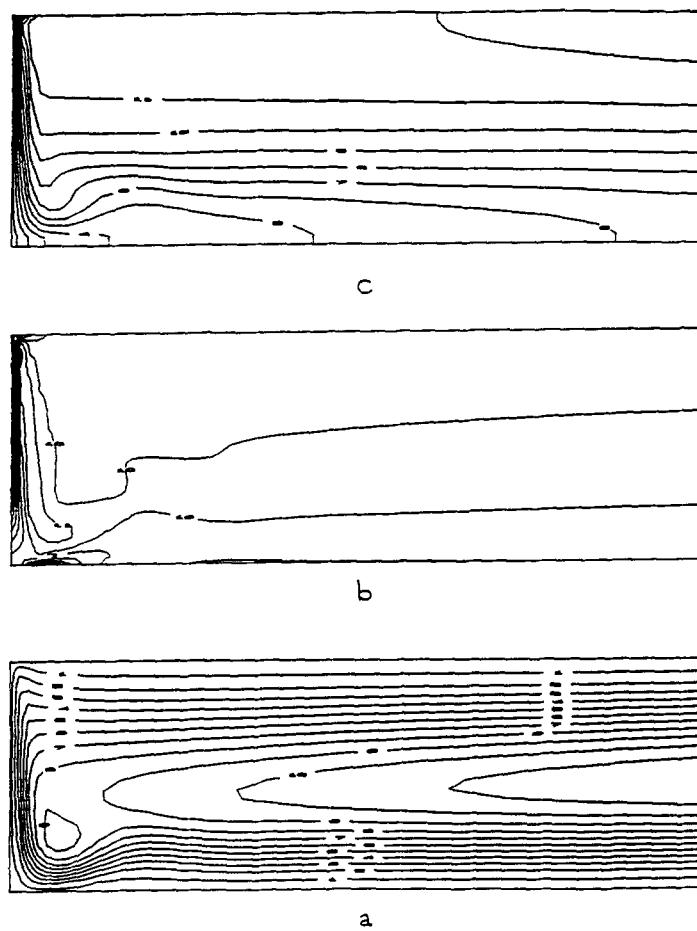

Fig. 7. Contours of the steady-state solution for (a) stream function, (b) vorticity, (c) temperature, for $\sigma = 0.733$ and $R_1 = 14\,000$, using a 175×25 grid with $x_\infty = 7$.

where, for $\sigma = 0.733$, $f''(0) \approx 0.897$. In Figure 11 the right-hand side of (34) with c_0 given by (33) is compared with the computed values of the left-hand side for each Rayleigh number. This suggests that the Rayleigh number scaling is correct and the quantitative comparison appears to be reasonable for the top half of the vertical boundary layer. The discrepancy in the bottom half is thought to be due to the corner structure at the bottom of the cold wall which may only be attained for extremely high Rayleigh numbers if the type of structure envisaged by Smith and Duck [27] is valid there. The present computations indicate the right trend but results need to be obtained for much higher Rayleigh numbers to confirm the asymptotic predictions.

For the heat transfer, the boundary-layer theory predicts a form proportional to R_1^2 as $R_1 \to \infty$, or more specifically

$$R_1^{-2} \left. \frac{\partial T}{\partial x} \right|_{x=0} \to \lambda c_0^{5/4} (1 - z)^{-1/4}, \quad R_1 \to \infty, \tag{35}$$

where λ is given by (26). In Figure 12 the right-hand side of (35) with c_0 given by (33) is

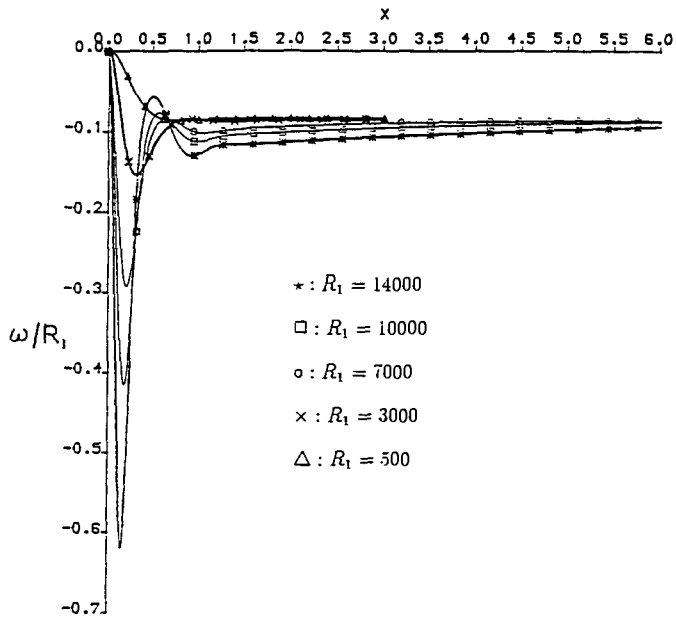

Fig. 8. Skin friction ω/R_1 on the bottom wall with $\sigma = 0.733$ for various Rayleigh numbers.

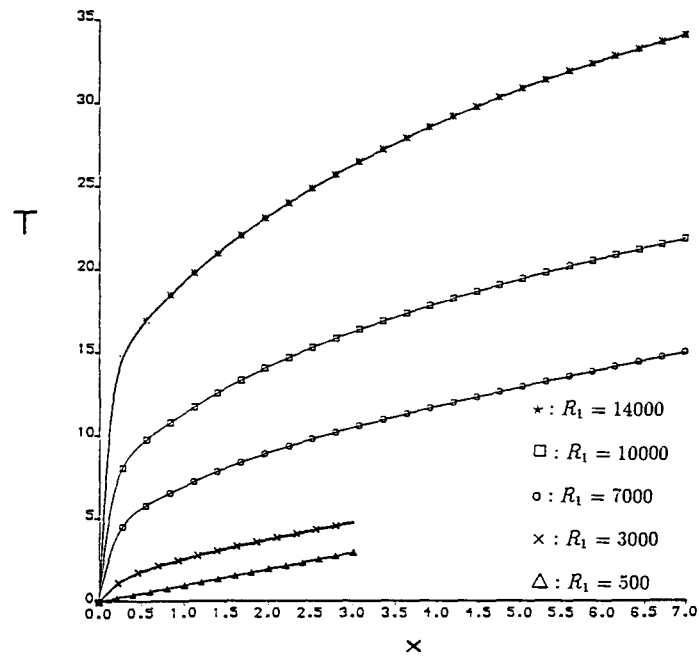

Fig. 9. Temperature T on the bottom wall with $\sigma = 0.733$ for various Rayleigh numbers.

compared with the computed values of the left-hand side for each Rayleigh number. Again this suggests that the Rayleigh number scaling is correct and the comparison for the region $z \geqslant 0.3$ is quite convincing. Again the corner structure may be responsible for the discrepancy observed in the region close to $z = 0$.

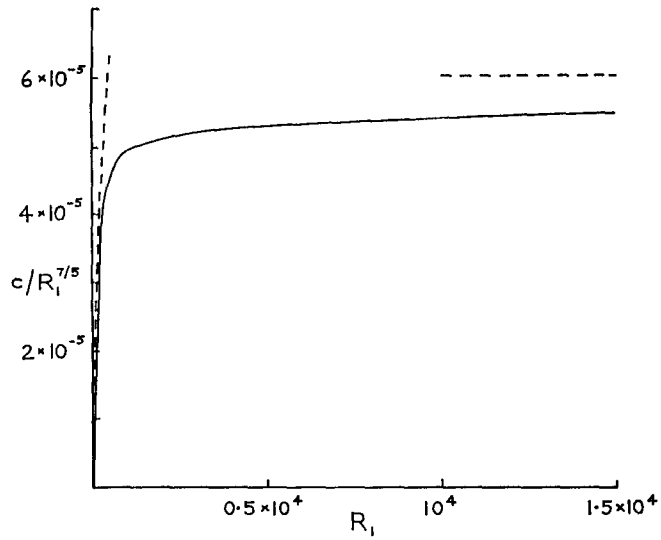

Fig. 10. Numerical computation of the parameter c for $\sigma = 0.733$, and the asymptotes predicted by (23) and (29) (– – –).

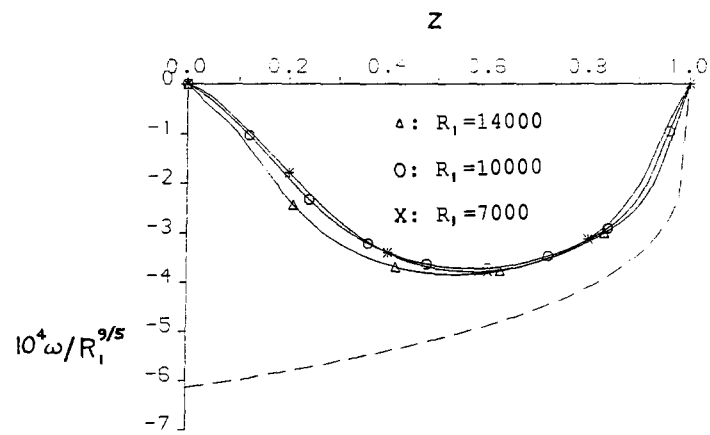

Fig. 11. Scaled skin friction $\omega/R_1^{9/5}$ on the cold wall with $\sigma = 0.733$ for various Rayleigh numbers and the asymptotic profile predicted by boundary-layer theory (– – –).

Other general features of the computations at high Rayleigh numbers are encouraging in terms of the proposed asymptotic structure. Apart from the vertical boundary-layer structure, the asymptotic theory predicts that the flow must turn the corner at the base of the cold wall and then develop within a horizontal layer where the isotherms descending the cold wall attach to the bottom wall of the cavity. The horizontal structure eventually merges with the main recirculatory flow in the end zone on the long scale $x = O(R_1)$ as $R_1 \to \infty$. This scale is observed in the numerical computations and the isotherm pattern of Figure 7 is consistent with the expected behaviour.

Results have also been obtained for the case of water ($\sigma = 6.983$). At low Rayleigh numbers the flow patterns are similar to those of air, [23]. More work is needed to obtain results for high Rayleigh numbers to compare with the asymptotic theory in this case.

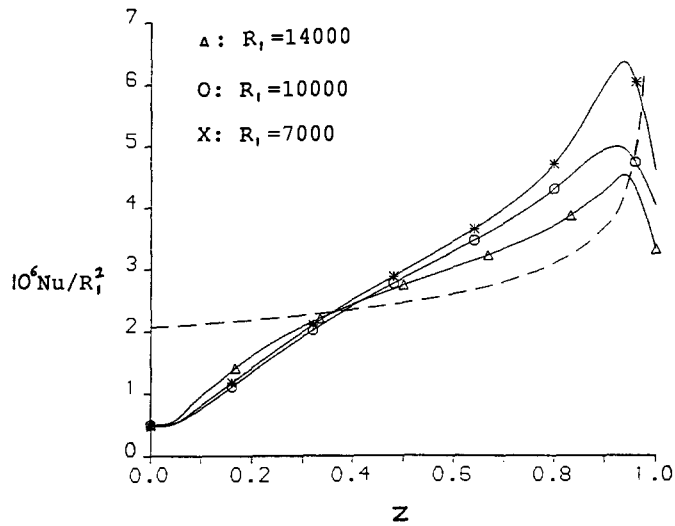

Fig. 12. Scaled local Nusselt number Nu/R_1^2 on the cold wall with $\sigma = 0.733$ for various Rayleigh numbers and the asymptotic profile predicted by boundary-layer theory (– – –).

6. Discussion

A detailed numerical study of the end zone in a shallow cavity with insulated horizontal boundaries has been carried out. For low Prandtl number fluids, secondary flow is seen to appear in the form of stationary transverse rolls in agreement with the predictions of linear stability theory and the earlier computations reported in [8]. At low Rayleigh numbers the present computation of the parameter c in the temperature field of the core flow is in good agreement with the theoretical prediction of c in [4], while at high Rayleigh numbers the numerical solutions for air are in good agreement with the theoretical prediction of c based on boundary-layer theory [11]. Computations of the skin friction and heat transfer at the cold wall also appear to be consistent with the Rayleigh-number dependence predicted by boundary-layer theory although the computations need to be extended to much higher Rayleigh numbers in order to confirm this and to adequately test the detailed functional dependence on z. In the future it is hoped to use a more sophisticated computational scheme to perform accurate numerical calculations at Rayleigh numbers $R_1 \geqslant 20\,000$, taking proper account of the various short and long length scales involved in this complex high Rayleigh number flow.

One of us (P. Wang) is grateful for support in the form of an Overseas Research Studentship.

References

1. D.T.J. Hurle, E. Jakeman and C. Johnson, Convective temperature oscillations in molten gallium. *J. Fluid Mech.* 64 (1974) 565–576.
2. B.E. Boyack and D.W. Kearney, Heat transfer by laminar natural convection in low aspect ratio cavities. *ASME Paper* 72-HT-2 (1972).

3. A. Bejan and A.N. Rossie, Natural convection in a horizontal duct connecting two fluid reservoirs. *J. Heat Transfer* 103 (1981) 108–113.
4. D.E. Cormack, L.G. Leal and J. Imberger, Natural convection in a shallow cavity with differentially heated end walls. Part 1. Asymptotic theory. *J. Fluid Mech.* 65 (1974) 209–229.
5. J. Imberger, Natural convection in a shallow cavity with differentially heated end walls. Part 3. Experimental results. *J. Fluid Mech.* 65 (1974) 247–260.
6. A. Bejan, A.A. Al-Homoud and J. Imberger, Experimental study of high Rayleigh number convection in a horizontal cavity with different end temperatures. *J. Fluid Mech.* 109 (1981) 283–299.
7. P.G. Simpkins and K.S. Chen, Convection in horizontal cavities. *J. Fluid Mech.* 166 (1986) 21–39.
8. J.E. Hart, Low Prandtl number convection between differentially heated end walls. *Int. J. Heat Mass Transfer* 26 (1983) 1069–1074.
9. P.G. Daniels, P.A. Blythe and P.G. Simpkins, Onset of multicellular convection in a shallow laterally heated cavity. *Proc. Roy. Soc. Lond.* A411 (1987) 327–350.
10. J.E. Hart, Stability of thin non-rotating Hadley circulations. *J. Atmos. Sci.* 29 (1972) 687–697.
11. P.G. Daniels, High Rayleigh number thermal convection in a shallow laterally heated cavity. *Proc. Roy. Soc. Lond.* A440 (1993) 273–289.
12. A.E. Gill, The boundary layer regime for convection in a rectangular cavity. *J. Fluid Mech.* 26 (1966) 515–536.
13. P.J. Roache, *Computational Fluid Dynamics*. Hermosa, New Mexico (1976).
14. A. Brandt, Multi-level adaptive solutions to boundary-value problems. *Math. Comp.* 31 (1977) 333–390.
15. E. Pohlhausen, Der Warmeaustausch zwischen festen Korpern und flussigkeiten mit kleiner Reibung und Warmeleitung. *Z. Angew Math. Mech.* 1 (1921) 115–121.
16. S. Ostrach, *An analysis of laminar free convection flow and heat transfer about a flat plate parallel to the direction of the generating body force*. N.A.C.A. Tech. Note 2635, Washington D.C. (1952).
17. P.G. Daniels and R.J. Gargaro, Numerical and asymptotic solutions for the thermal wall jet. *J. Eng. Math.* 26 (1992) 493–508.
18. P.G. Daniels and R.J. Gargaro, Buoyancy effects in stably-stratified horizontal boundary-layer flow. *J. Fluid Mech.* 250 (1993) 233–251.
19. J. Crank and P. Nicolson, A practical method for numerical evaluation of solutions of partial differential equations of the heat-conduction type. *Proc. Camb. Phil. Soc.* 43 (1947) 50–67.
20. D.W. Peaceman and H.H. Rachford, The numerical solution of parabolic and elliptic differential equations. *J. Sco. Indust. Appl. Math.* 3 (1955) 28–41.
21. J.E. Drummond, *A numerical study of natural convection in shallow cavities*. PhD thesis, Ohio State Univ. (1981).
22. A. Arakawa, Computational design for long-term numerical integration of the equations of fluid motion: two dimensional incompressible flow, part 1. *J. Comp. Phys.* 1 (1966) 119–143.
23. P. Wang, *Thermal convection in slender laterally-heated cavities*. PhD thesis, City University (1992).
24. D.E. Cormack, L.G. Leal and J.H. Seinfeld, Natural convection in a shallow cavity with differentially heated end walls. Part 2. Numerical solutions. *J. Fluid Mech.* 65 (1974) 231–246.
25. K. Kublbeck, G.P. Merker and J. Straub, Advanced numerical computation of two-dimensional time-dependent free convection in cavities. *Int. J. Heat Mass Transfer* 23 (1980) 203–217.
26. J.E. Drummond and S.A. Korpela, Natural convection in a shallow cavity. *J. Fluid Mech.* 182 (1987) 543–564.
27. F.T. Smith and P.W. Duck, Separation of jets or thermal boundary layers from a wall. *Q.J. Mech. Appl. Math.* 30 (1977) 143–156.